

Probing specific RNA bulge conformations by modified fluorescent nucleosides†

Hyun Seok Jeong,^{a,b} Sunwoo Kang,^c Jin Yong Lee^{*c} and Byeang Hyeon Kim^{*a}

Received 24th September 2008, Accepted 28th November 2008

First published as an Advance Article on the web 23rd January 2009

DOI: 10.1039/b816768k

Recently, RNA bulges, three-dimensional structural motifs that function as molecular handles in RNA, were identified in various sequences and have been proposed as the interaction site for RNA-binding drugs. However direct and sensitive monitoring methods specific to RNA bulges have not been well developed. We describe here pyrene-labeled uridine derivatives which were incorporated into HIV TAR RNA bulge sites resulting in greatly enhanced fluorescence, allowing the effective monitoring of base conformations in HIV TAR RNA. To clarify this fluorescence enhancement, Hartree–Fock calculations were performed for natural and pyrene-labeled HIV TAR RNA. The calculated results showed a considerable rotation of the pyrene moiety at U25 due to argininamide-induced conformational changes in the RNA bulge. This simple and efficient method can be used to elucidate conformational changes in specific bulge regions.

Introduction

RNA bulges are common and recurring motifs in three-dimensional structures in RNA. They consist of unpaired bases typically located between stacked base pairs in duplex RNA to create unique recognition sites.¹ Recently, RNA bulges were discovered in various RNA structures such as HIV trans-activator responsive (TAR) RNA, RNA splicing intermediates, and 5S ribosomal RNA.² Bulge structures are highly conserved and function as molecular handles or specific binding sites by widening or compressing RNA grooves. Consequently, RNA bulges can be a spotlighting target of RNA binding drugs.³

RNA bulge conformation may be stacked or unpaired, oriented into the groove or as flap residues.⁴ Therefore to quickly characterize a bulge and its interactions, it is important to develop effective and simple means of monitoring RNA bulge conformations. Although several approaches have emerged,⁵ a direct and sensitive method is lacking. In this study, a new method for monitoring RNA bulge conformation was developed using a fluorescent nucleoside based on reasonable *ab initio* Hartree–Fock (HF) calculations.

In the free HIV TAR RNA, bulge residues at U23 RNA base and U25 RNA base are stacked in the RNA groove, but when argininamide binds to RNA, both U23 RNA base and U25 RNA base undergo considerable changes due to ligand–RNA interactions.⁷

HIV TAR RNA is known to contain specific RNA bulge sites (UCU) that specifically interact with Tat protein, an essential factor for viral replication.⁶ This interaction can be reduced to its components, the HIV TAR RNA bulge and a Tat peptide mimic, argininamide (ARG).

To monitor these conformational changes, we incorporated a fluorescent nucleoside developed by our research group⁸ and other groups⁹ into an RNA nucleoside to yield a novel pyrene-labeled uridine nucleoside. Covalently linked ethynyl pyrene gives several important advantages. First, the ethynyl moiety at uridine C-5 is presumably a strong and stable bond that is not likely to perturb RNA base pairing or duplex stability.¹⁰ Second, the fluorophore pyrene is well characterized and sensitive to the hydrophobicity of its surrounding environment. Since the RNA bulge conformation depends on interactions with other stacked bases, the covalently bound ethynyl pyrene can be an effective means of probing RNA bulge residues.

Results and discussion

First, pyrene-labeled uridine phosphoramidite **5** was synthesized from 5-iodo-5'-dimethoxytrityl-2'-*tert*-butyldimethylsilyldimethyluridine **3** through a palladium-catalyzed Sonogashira coupling intermediate **4** (Fig. 1). The corresponding phosphoramidite was incorporated into HIV TAR RNA by automated RNA synthesis.

Three possible uridine RNA bulges can occur in HIV TAR RNA at U23, U25, and U31 (Fig 2a). As a control, an unmodified HIV TAR RNA **6** was synthesized in addition to the three RNA (U23, U25, U31) **7–9** including pyrene-labeled uridine (Fig. 2b) in site specific manners (Fig. 2c).

The fluorescence emission of the pyrene-labeled RNA bulge increased with the concentration of argininamide (Fig. 3a). The overall shape of the fluorescence spectra varied among the pyrene-labeled RNA bulges due to different stacking arrangements with the RNA bases. Specifically, the fluorescence intensity of pyrene-labeled U25-RNA **8** increased approximately 6.2 fold with the

^aDepartment of Chemistry, BK School of Molecular Science, Pohang, 790-784, Korea

^bSchool of Interdisciplinary Bioscience and Bioengineering (I-BIO), Pohang University of Science and Technology, Pohang, 790-784, Korea. E-mail: bhkim@postech.ac.kr

^cDepartment of Chemistry, Institute of Basic Science, Sungkyunkwan University, Suwon, 440-746, Korea

† Electronic supplementary information (ESI) available: The initial structures for each modeling complex, ¹H NMR spectra for compound **2–5**, and MALDI-TOF data and MALDI-TOF spectra for synthesized RNA **6–9**. See DOI: 10.1039/b816768k

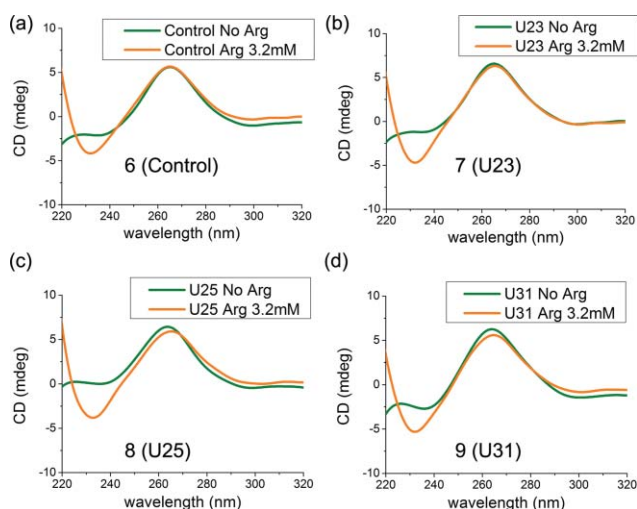


Fig. 5 Circular dichroism spectra of natural (green) and modified ODNs (orange). The spectra were recorded at 20 °C in a buffer of 100 mM Tris-HCl, 100 mM NaCl (pH 7.2) with or without 3.2 mM of argininamide (ARG). Each natural and modified ODNs concentration was 1 μ M.

using a STO-3G basis set in Gaussian 03 software¹¹ (Fig. 6) in the gas phase. Due to limited computational capabilities, a simplified model composed of seven base pairs and one bulge site was employed to mimic entire HIV TAR RNA to precisely simulate its interaction with argininamide. Several argininamide units can bind with HIV TAR RNA, however the specific argininamide which binds to the specific RNA bulge site was mainly considered.

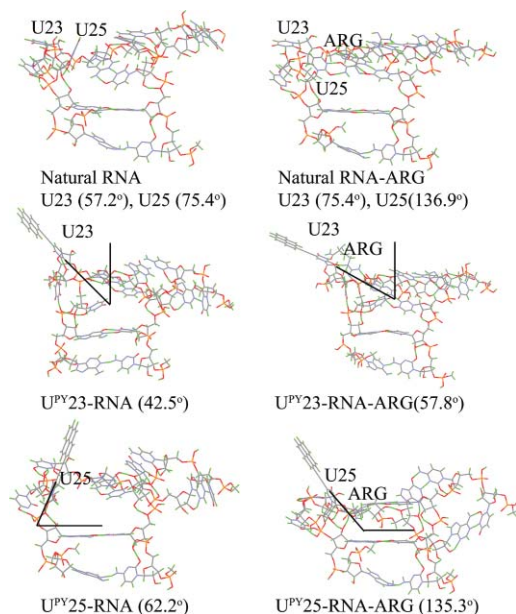


Fig. 6 The optimized structures of natural RNA, natural RNA-ARG, U^{PY}23-RNA, U^{PY}25-RNA, U^{PY}23-RNA-ARG, and U^{PY}25-RNA-ARG providing dihedral angle values.

In addition, the pyrene moiety is hydrophobic and the water-pyrene interaction should be small. The pyrene-RNA interactions in water solution may be different from the pyrene-RNA interactions in the gas phase. However, such hydrophobic interactions

in bulk and not in molecule-molecule interactions cannot be considered even in the current *ab initio* calculations based on self-consistent reaction field (SCRf) methods because the main origin of the hydrophobic interaction is the entropic contribution by forming a huge cavity in solvent water, which can not be considered in current *ab initio* calculations. The pyrene-RNA interactions calculated in the gas phase may change in water solution, which gives the enthalpic contribution. In our previous studies on enzyme reactions, the enzyme-substrate interaction was often electrostatic (dipole-dipole interaction) in the hydrophobic pocket (active sites) and the gas phase results gave reliable results. This electrostatic interaction in a hydrophobic pocket is the reverse of the current case of hydrophobic interactions in water solution, thus our calculations in the gas phase can give reasonable conclusions even though the pyrene-RNA interaction may change in water solution.

The modification effect of pyrene labeling at each bulge was estimated by the rotation angles at U23 and U25 bases. The changes in the dihedral angle between natural RNA and pyrene modified RNA were about 15° at U23 (57.2° in natural RNA **6**, 42.5° in U^{PY}23-RNA **7**) and U25 (75.4° in natural RNA **6**, 62.2° in U^{PY}25-RNA **8**). These values showed that pyrene labeling of an RNA base did not change the RNA base orientations and maintained the original RNA base orientations. The next calculated results indicated that the binding of argininamide induced a major shift in the rotational position of pyrene and a net movement of the pyrene moiety away from the RNA base pair backbone. The change in the dihedral angle of pyrene in U^{PY}25-RNA upon argininamide binding (73.1°) was much larger than the corresponding change for U^{PY}23-RNA (15.3°). These results clearly support the observed fluorescence enhancement of U^{PY}25-RNA upon argininamide binding. In addition, the change in the dihedral angle of natural RNA showed similar changes in the uridine base at U23 (18.2°) and U25 (61.5°) compared to pyrene labeled RNA. Therefore pyrene labeling has little effect on RNA local structures, it does not change much the rotation angles upon argininamide binding. The initial and optimized structures for each structures are shown in the ESI.†

In HIV TAR RNA without argininamide, fluorescence from pyrene-labeled RNA uridine is quenched by interactions with adjacent base pairs through photo-induced electron transfer (PET).¹² Since RNA bulge sites are typically intercalated in base pair stacks, ligands or proteins that bind at the bulge site can decrease base pair stacking, thereby exposing buried RNA residues. When argininamide binds with HIV TAR RNA, the U25 base is reoriented outside of the RNA groove, diminishing base pair quenching effects and resulting in increased fluorescence with a strongly emissive pyrene.

The fluorescence of the covalently linked ethynyl pyrene described herein is sensitive to these changes in base interaction and can be a useful tool to measure RNA bulge conformation. This technique provides several advantages. First, base pair orientational changes can be measured, since conformational changes in RNA bulges depend on base pair orientation. Second, the environment surrounding the uridine base to which the ethynyl pyrene moiety is attached is probed directly. Similar results were obtained using 2'-amino-butryl-pyrene uridine with the pyrene moiety attached at the 2'-hydroxyl group of sugar ring.¹³ Third, relative to NMR spectroscopy, the use of a labeled nucleoside

represents a much simpler and more efficient probing method. Fourth, compared to other monitoring methods,¹⁴ the sensitivity of pyrene-labeled uridine affords detection of minute structural, conformational, and orientational changes in RNA bulges.

Conclusions

In conclusion, a pyrene-labeled uridine derivative was synthesized by Sonogashira coupling to probe base pair conformation and stacking interactions in RNA bulges. The fluorescence discriminating factors of the pyrene moiety were so high that it is sufficient to detect changes in RNA base conformations, for example, in HIV TAR RNA with argininamide. Pyrene labeling of RNA has a minimum effect on RNA natural structures and the modeling results of pyrene labeled RNA upon argininamide binding were consistent with natural RNA modeling results upon the same case. Therefore this monitoring method can be used to detect and characterize conformational changes in RNA or DNA bulge regions due to targeted binding events such as RNA binding protein or drug interactions.

Experimental section

5'-O-[Bis(4-methoxyphenyl)phenylmethyl]-5-iodouridine (2)

4,4'-Dimethoxytrityl chloride (704 mg, 2.08 mmol) was added to a solution of (–)-5-iodouridine (700 mg, 1.89 mmol) and 4-dimethylaminopyridine (26 mg, 0.21 mmol) in pyridine (10 mL). After stirring at room temperature for 3 h, the mixture was concentrated under reduced pressure. A 5% NaHCO₃ solution (10 mL) was added to the mixture, and the solution was extracted with ethyl acetate 2 times (10 mL), and then dried with sodium sulfate. Column chromatography (SiO₂; hexane–ethyl acetate, from 1 : 1 for eliminating pyridine, to 1 : 4) gave product **2** as a white solid in 83% yield. [α]_D²⁰ = +12 (CHCl₃). IR (film): ν 3400, 3065, 2930, 2835, 1699, 1607, 1508, 1445, 1301, 1250, 1220, 1175, 1095, 1054, 1033, 828, 771, 723, 700, 667 cm⁻¹. ¹H NMR (300 MHz, CDCl₃): δ 8.23 (s, 1H; H₆), 7.19–7.39 (m, 9H; DMT), 6.84–6.80 (d, J = 8.7 Hz, 4H; DMT), 5.86 (s, 1H; H₁) 4.46 (t, J = 4.80 Hz, 1H; H₂), 4.36 (q, 1H, J = 3.94 Hz; H₃) 4.24 (br s, 1H; H₄), 3.75 (s, 6H, OCH₃), 3.42 (d, J = 9.2 Hz, 2H; H_{5'}), 3.36 (d, 2H, J = 9.2 Hz, H5''). ¹³C NMR (75 MHz, CDCl₃): δ 160.1, 158.2, 150.6, 143.9, 135.0, 134.8, 129.6, 127.7, 127.5, 126.6, 112.9, 90.1, 86.5, 84.2, 75.1, 70.4, 68.5, 66.3, 62.4 54.8. FAB (m/z): [M + Na]⁺ calcd for C₃₀H₂₉IN₂O₈Na, 695.09; found, 695.09.

5'-O-[Bis(4-methoxyphenyl)phenylmethyl]-2'-O-(tert-butyl-dimethylsilyl)-(–)-5-iodouridine (3)

Dry pyridine (0.36 mL, 4.76 mmol) was added to a solution of product **2** (600 mg, 0.892 mmol) and silver nitrate (182 mg, 1.07 mmol) in dry THF (10 mL). The reaction mixture was stirred at room temperature for 15 min, followed by the addition of *tert*-butyldimethylsilyl chloride (175 mg, 1.16 mmol). Stirring for an additional 2 h, the solution was extracted with 5% NaHCO₃ solution and ethyl acetate and dried with sodium sulfate. Column chromatography (SiO₂; hexane–ethyl acetate, 2 : 1) gave product **3** as a white solid in 66% yield. [α]_D²⁰ = +16 (CHCl₃). IR (film): ν 3464, 3064, 2929, 2956, 1700, 1609, 1507, 1456, 1251, 1219, 1177, 1135, 1091, 1034, 837, 772, 668 cm⁻¹. ¹H NMR (300 MHz,

CDCl₃): δ 8.20 (s, 1H; H₆), 7.24–7.41 (m, 9H; DMT), 6.85–6.82 (d, J = 8.7 Hz, 4H; DMT), 5.98 (s, 1H; H₁) 4.48 (t, J = 4.80 Hz, 1H; H₂), 4.24 (q, 1H, J = 3.94 Hz; H₃) 4.16 (br s, 1H; H₄), 3.78 (s, 6H, OCH₃), 3.44 (d, J = 9.2 Hz, 2H; H_{5'}), 3.38 (d, 2H, J = 9.2 Hz, H5''). 0.91 (s, 9H, *t*-butyl). ¹³C NMR (75 MHz, CDCl₃): δ 158.2, 149.3, 143.8, 134.8, 134.7, 129.6, 127.7, 127.5, 126.7, 112.9, 87.6, 86.8, 83.6, 71.0, 62.7, 54.9, 25.1, 17.5. FAB (m/z): [M + Na]⁺ calcd for C₃₆H₄₃IN₂O₈SiNa, 809.17; found, 809.05.

5'-O-[Bis(4-methoxyphenyl)phenylmethyl]-2'-O-(tert-butyl-dimethylsilyl)-5-(2-pyrenylethynyl)uridine (4)

(PPh₃)₄Pd (18 mg, 0.015 mmol) and CuI (6 mg, 0.031 mmol) were added to a solution of **3** (240 mg, 0.305 mmol) in THF under Ar and then the mixture was stirred for 5 min at room temperature. 1-Ethynylpyrene (83 mg, 0.366 mmol) was added to this solution. After degassing, the reaction mixture was stirred at 45 °C for 5 h and monitored by TLC. Water was added to the solution and the product was extracted with excess ethyl acetate. The organic phase was washed twice with water. After evaporation of solvent under reduced pressure, the residue was subjected to column chromatography (SiO₂; hexane–ethyl acetate, 2 : 1) to yield product **4** (254 mg, 94%). [α]_D²⁰ = +16 (CHCl₃). IR (film): ν 3460, 3200, 3033, 2929, 2856, 1717, 1616, 1506, 1457, 1252, 1218, 848, 772 cm⁻¹. ¹H NMR (300 MHz, CDCl₃): δ 8.41 (d, J = 9.2 Hz, 1H; Ar_{py}H), 8.30 (s, 1H; H₆), 8.14 (t, J = 6.8 Hz, 2H; Ar_{py}H), 8.03 (d, J = 8.0 Hz, 1H, Ar_{py}H), 7.98 (d, J = 8.3, 5.4 Hz, 2H; Ar_{py}H), 7.89 (t, J = 8.0 Hz, 2H; Ar_{py}H) 7.56 (d, J = 8.0 Hz, 1H; Ar_{py}H) 7.41–7.24 (m, 9H; DMT), 6.68–6.64 (d, J = 8.7 Hz, 4H; DMT), 6.09 (s, 1H; H₁), 4.41 (t, J = 4.80 Hz, 1H; H₂), 4.11 (br s, 1H; H₄), 4.09 (q, 1H, J = 3.94 Hz; H₃), 3.63 (d, J = 9.2 Hz, 2H; H_{5'}), 3.49 (s, 3H, OCH₃), 3.43 (s, 3H, OCH₃), 3.40 (d, 2H, J = 9.2 Hz, H5''). 0.93 (s, 9H, *t*-butyl). ¹³C NMR (75 MHz, CDCl₃): δ 160.1, 158.1, 148.8, 144.0, 134.9, 130.8, 131.0, 130.0, 129.9, 129.6, 128.0, 127.7, 127.4, 126.7, 125.6, 125.1, 125.0, 123.7, 125.5, 112.9, 101.3, 87.8, 87.0, 83.4, 71.1, 62.7, 60.0, 54.5, 25.1, 17.6. FAB (m/z): [M + Na]⁺ calcd for C₅₄H₅₂N₂O₈SiNa, 908.44; found, 908.44.

5'-O-[Bis(4-methoxyphenyl)phenylmethyl]-2'-O-(tert-butyl-dimethylsilyl)-5-(2-pyrenylethynyl)uridine 3'-O-[2-cyanoethyl(*N,N*-diisopropylamino)phosphoramidite (5)

4-Methylmorpholine (74 mL, 0.678 mmol) was added to a solution of product **3** (100 mg, 9.113 mmol) in CH₂Cl₂ (5 mL) under nitrogen and then the mixture was stirred at room temperature for 30 min. 2-Cyanoethyl-diisopropyl-aminochlorophosphoramidite (76 mL, 0.339 mmol) was added and the mixture was stirred for 3 h and monitored by TLC. The solvent was washed with 5% NaHCO₃ and the residue was purified by chromatography on short column (SiO₂; hexane–EtOAc–pyridine, 99 : 99 : 2) to yield product **4** (85%). [α]_D¹⁴ = +15 (CHCl₃). IR (film): ν 3177, 3015, 2970, 2950, 1733, 1616, 1507, 1456, 1365, 1294, 1217, 1179, 1093, 1034, 846, 772 cm⁻¹. ¹H NMR (300 MHz, CDCl₃): δ 8.41 (s, 1H; H₆), 8.38–8.35 (d, J = 9.2 Hz, 1H; Ar_{py}H), 8.14 (t, J = 6.8 Hz, 2H; Ar_{py}H), 8.03 (d, J = 8.0 Hz, 1H, Ar_{py}H), 8.00 (d, J = 8.3, 5.4 Hz, 2H; Ar_{py}H), 7.86 (t, J = 8.0 Hz, 2H; Ar_{py}H) 7.67 (d, J = 8.0 Hz, 1H; Ar_{py}H) 7.50–7.24 (m, 9H; DMT), 6.74–6.68 (d, J = 8.7 Hz, 4H; DMT), 6.10 (s, 1H; H₁), 4.26 (t, J = 4.80 Hz, 1H; H₂), 4.21 (br s, 1H; H₄), 4.09 (q, 1H, J = 3.94 Hz; H₃), 3.88–3.45 (m, 5H,

NCH₂, OCH₂, H₅'), 3.49 (s, 3H, OCH₃), 3.43 (s, 3H, OCH₃), 3.40 (d, 2H, $J = 9.2$ Hz, H₅'). 2.71 (m, 2H, CH₂CN), 1.24–1.15 (2d, 12H, $J = 6.8$ Hz; NCHCH₃), 0.93 (s, 9H, t-butyl). ¹³C NMR (75 MHz, CDCl₃): δ 160.1, 158.2, 149.3, 144.0, 141.2, 143.8, 134.8, 134.7, 129.6, 127.7, 127.5, 126.7, 112.9, 100.6, 87.6, 86.8, 83.6, 71.0, 62.7, 54.9, 42.8, 30.5, 25.1, 19.7, 17.5. ³¹P NMR (121 MHz, CDCl₃): δ 152.1, 150.3. FAB (m/z): $[M + Na]^+$ calcd for C₃₆H₄₃IN₂O₈SiNa, 809.17; found, 809.05.

RNA oligonucleotide synthesis and characterization

To synthesize modified RNA oligonucleotides, we prepared the DMTr-protected 2-cyanoethyl phosphoramidite derivative and applied it directly into solid phase oligonucleotide synthesis protocols using an automated DNA synthesizer, Perceptive Biosystems 8909 Expedite™. The synthesized oligonucleotides were cleaved from the solid support upon treatment with MeNH₂ in H₂O–EtOH = 3 : 1 for 5 h at room temperature. The crude products were lyophilized and diluted with 1-methyl-2-pyrrolidone–triethylamine–TEA–HF = 6 : 3 : 4 to remove the protecting 2'-TBDMS group. After heating the solution for 2 h at 65 °C, the solution was neutralized with TBE solution. The oligonucleotides were purified using HPLC (Hiber Pre-packed Column RT 250–10, customized packing Lichrospher 100 RP-18). The HPLC mobile phase was the gradient between 5% acetonitrile–0.1 M triethylammonium acetate (TEAA) (pH 7.0) and 50% acetonitrile–0.1 M TEAA at 2.5 mL min⁻¹. The fractions containing oligonucleotides were checked by UV and collected. The collected solution was treated by 1 M NaOAc–AcOH solution to remove the 5'-DMTr group. The purified oligonucleotides were precipitated with 3 M NaOAc–AcOH solution and excess EtOH. Final products were obtained by desalting of the solution using an NAP-10 Column (Amersham Bioscience). For characterization of oligonucleotides, matrix-assisted laser desorption ionization time-of-flight (MALDI-TOF) mass spectroscopy was used.

The calculation of dihedral angle values of RNA

The dihedral angle values of natural RNA, natural RNA-ARG, U^{PY}23-RNA, U^{PY}25-RNA, U^{PY}23-RNA-ARG, and U^{PY}25-RNA-ARG were obtained from optimized structures using a dot product equation, $\mathbf{A} \cdot \mathbf{B} = |\mathbf{A}||\mathbf{B}|\cos\theta$. Then, each angle was obtained by $\theta = \cos^{-1}(\mathbf{A} \times \mathbf{B} / |\mathbf{A}||\mathbf{B}|)$, where vectors \mathbf{A} and \mathbf{B} are given in the black lines in Fig 6.

Acknowledgements

BHK is grateful to KOSEF for financial support through CRI-Acceleration Research grant by MEST (No. R21-2008-035-0100-0). JYL acknowledges the KOSEF grant by MEST (No. R11-2007-012-03002-0).

Notes and references

- 1 T. Hermann and D. J. Patel, *Structure*, 2000, **8**, R47–R54.
- 2 F. Aboul-ela, J. Karn and G. Varani, *Nucleic Acids Res.*, 1996, **24**, 3974–3981; H. Huthoff, F. Girard, S. S. Wijmenga and B. Berkhout, *RNA*, 2004, **10**, 412–423; P. W. Huber, J. P. Rife and P. B. Moore, *J. Mol. Biol.*, 2001, **312**, 823–832.
- 3 A. I. H. Murchie, B. Davis, C. Isel, M. Afshar, M. J. Drysdale, J. Bower, A. J. Potter, I. D. Starkey, T. M. Swarbrick, S. Mirza, C. D. Prescott, P. Vaglio, F. Aboul-ela and J. Karn, *J. Mol. Biol.*, 2004, **336**, 625–638.
- 4 P. N. Borer, Y. Lin, S. Wang, M. W. Roggenbuck, J. M. Gott, O. C. Uhlenbeck and I. Pelczer, *Biochemistry*, 1995, **23**, 6488–6503; S. Portmann, S. Grimm, C. Workman, N. Usman and M. Egli, *Chem. Biol.*, 1996, **3**, 173–184; N. L. Greenbaum, I. Radhakrishnan, D. J. Patel and D. Hirsh, *Structure*, 1996, **4**, 725–733; E. Ennifar, M. Yusupov, P. Walter, R. Marquet, B. Ehresmann, C. Ehresmann and P. Dumas, *Structure*, 1999, **7**, 1439–1449.
- 5 A. Lapidot, V. Vijayabaskar, A. Litovchick, J. Yu and T. L. James, *FEBS Lett.*, 2004, **577**, 415–421; Y. Xiong, J. Deng, C. Sudarsanakumar and M. Sundaralingam, *J. Mol. Biol.*, 2001, **313**, 573–582; J. Zhang, F. Takei and K. Nakatani, *Bioorg. Med. Chem.*, 2007, **15**, 4813–4817.
- 6 P. A. Sharp and R. A. Marciniak, *Cell*, 1989, **59**, 229–230.
- 7 K. S. Long and D. M. Crothers, *Biochemistry*, 1999, **38**, 10059–10069; Q. Zhang, X. Sun, E. D. Watt and H. M. Al-Hashimi, *Science*, 2006, **311**, 653–656.
- 8 N. Venkatesan, Y. J. Seo and B. H. Kim, *Chem. Soc. Rev.*, 2008, **37**, 648–663; Y. J. Seo, Rhee, T. Joo and B. H. Kim, *J. Am. Chem. Soc.*, 2007, **129**, 5244–5247; G. T. Hwang, Y. J. Seo and B. H. Kim, *Tetrahedron Lett.*, 2005, **46**, 1475–1477; Y. J. Seo and B. H. Kim, *Chem. Commun.*, 2006, 150–152; Y. J. Seo, I. J. Lee, J. W. Yi and B. H. Kim, *Chem. Commun.*, 2007, 2817–2819.
- 9 C. Wanniner-Weib, L. Valis and H. A. Wagenknecht, *Bioorg. Med. Chem.*, 2008, **16**, 100–106; M. Nakamura, Y. Shimomura, Y. Ohtoshi, K. Sasa, H. Hayashi, H. Nakano and K. Yamana, *Org. Biomol. Chem.*, 2007, **5**, 1945–1951; A. Okamoto, K. Kanatani and I. Saito, *J. Am. Chem. Soc.*, 2004, **126**, 4820–4827.
- 10 G. T. Hwang, Y. J. Seo and B. H. Kim, *J. Am. Chem. Soc.*, 2004, **126**, 6528–6529.
- 11 M. J. Frisch, *et al.*, *Gaussian 03, Revision A1*, Gaussian Inc., Pittsburgh, PA, 2003.
- 12 N. E. Geacintov, R. Zhao, V. A. Kuzmin, S. K. Kim and L. J. Pecora, *Photochemistry and Photobiology*, 1993, **58**, 185–194; M. Manoharan, K. L. Tivel, M. Zhao, K. Nafisi and T. L. Netzel, *Journal of Physical Chemistry*, 1995, **99**, 17461–17472; V. Y. Shafirovich, S. H. Courtney, N. Ya and N. E. Geacintov, *J. Am. Chem. Soc.*, 1995, **117**, 4920–4929.
- 13 K. F. Blount and Y. Tor, *Nucleic Acids Res.*, 2003, **31**, 5490–5500.
- 14 T. D. Bradrick and J. P. Marino, *RNA*, 2004, **10**, 1459–1468; S. G. Srivatsan and Y. Tor, *Tetrahedron*, 2007, **63**, 3601–3607.